International Research Journal of Engineering and Technology (IRJET) e-ISSN: 2395-0056
Volume: 09 Issue: 06 | June 2022 www.irjet.net p-ISSN: 2395-0072

A Novel Framework For Preprocessing Of Breast Ultra Sound Images By Combining Non-Local Means Filter For Speckle Noise Reduction And Morphological Operations For Image Enhancement

Rethy P V [1], Priya S [2] , Janu R Panicker [3] and Lekshmi R Nair [4]

[1] Department of Computer Engineering, Government Polytechnic College, Cherthala, India
[2,3,4] Department of Computer Engineering, College of Engineering, Cherthala, India

---

Abstract - *Ultrasound is one of the diagnostic methods used in breast cancer screening. Ultrasound patterns are known for being low-cost and non-invasive. The multiplicative speckle noise is a significant disadvantage of ultrasonography. Speckle noise reduces the usefulness of Breast Ultra Sound (BUS) images, lowering the test's efficiency. This research presents a new framework for reducing speckle noise and enhancing performance. The Non-Local Means (NLM) filter is used to minimize speckle noise, and then morphological techniques are used to enhance the noise-reduced BUS images. When tested on real BUS images, the model obtains a Peak Signal to Noise Ratio (PSNR) of 60 - 80 dB.*

Key words: Speckle noise, Breast Ultra Sound (BUS) images, ultrasonography, Non-Local Means (NLM) filter, Peak Signal to Noise Ratio (PSNR).

1.INTRODUCTION

Image analysis entails extracting essential details with the least amount of human interaction possible [1-3]. The function of medical imaging systems in image processing entails the use of semi-automated and fully automated algorithms for fast and accurate image analysis [4]. For the diagnosis of human diseases and ailments, such as tumor detection, a wide range of imaging modalities can be used. These gadgets are made to take images of human inside organs in a non-invasive manner. The ultrasound scan, often known as a sonogram, is one such instrument used for this purpose. It works by transmitting high-frequency sound waves via a bodily part's tissues. It features transducers that allow it to receive sound waves, which are then translated to electric impulses, allowing internal structural images to be displayed on a computer screen [5-6].

Machine learning, medical image classification methods, and pattern recognition methods must all be integrated into a multidisciplinary technology. To solve the obstacles connected with detecting and classifying gynecological disorders, this technology must be pursued in partnership with domain specialists. Because lifetime training helps professionals acquire a plethora of information, computer-based tools cannot replace human expertise. The hybrid technique is the most successful strategy for abnormality identification, and it can also improve patient care and management [7-9]. When creating a computer-based tool, it's critical to keep in mind why it's being created. This tool must either be created with features that aid decision-making, or it must be designed as standard software that facilitates the automatic extraction of features required by domain experts [10,11]. To create an intelligent decision support system model that can segment and identify the risks of malignant breast cancer early on, first identify the limits of existing approaches and try to mitigate their impacts. Ultrasound image restrictions can be divided into three categories. One of the key restrictions that can hinder segmentation and feature extraction is speckle noise. By raising false instances and lowering the clarity of the Region of Interest (RoI) edge, speckle noise reduces segmentation accuracy. Speckle noise has resulted in ambiguous ROI texture information, which can't be utilized to detect malignancy threats. As a result, creating or employing a suitable filter can help reduce speckle noise, making the work of segmentation and feature extraction much easier. Second, the artifact created by the machine can make segmentation challenging. Finally, powerful traits in determining the risk of malignancy may be difficult to come by. As a result, a model has been suggested that can be used to:

1. Reduce speckle noise with the help of Non-Local Means (NLM) filter.

2. Enhance the speckle noise-reduced images by applying various morphological treatments.

Before images are used in model training and inference, image preprocessing steps are required to format them. It

prepares the visual data for model input by cleaning it. It also cuts down on model training time and speeds up model inference. If the input images are very huge, shrinking them will considerably reduce model training time without compromising model performance.

2. Related Work

Various classical filters are used in all current works for BUS preprocessing. Deep learning was used for a portion of the study.

The median filter is a nonlinear denoising filter that is often used to remove noise from images[12]. Because of its efficacy and precision, it is the most widely utilized approach.

$$\text{median}[A(x) + B(x)] \neq \text{median}[A(x)] + \text{median}[B(x)] \quad (1)$$

From Equation 1, A(x) and B(x) are the original image and the noisy image respectively.

The adaptive median filter is applied to a rectangular area S_{xy}. During the filtering operation, it modifies the size of S_{xy} depending on the conditions given below. The median value in the 3-by-3 neighborhood around the corresponding pixel in the input images is stored in each output pixel. The images' edges, on the other hand, are replaced with zeros [13]. The filter's output is a single value that replaces the current pixel value at (x, y), where S is currently centered.

The average value of the intensities in each pixel's neighbourhood is substituted for each pixel using the mean filter [14]. In terms of mean square error, it has the effect of blurring and smoothing the image and is the best choice for additive Gaussian noise. The basic mean filter does not work in this situation because a speckled image is a multiplicative model with non-Gaussian noise [15].

The adaptive mean filters [14] have been developed to establish a balance between straightforward averaging in homogenous regions and all-pass filtering where there are edges in order to reduce the blurring effect. They locally adjust to the image's characteristics and remove speckles from particular areas of the image. They efficiently identify and maintain edges and features by using local image statistics including mean, variance, and spatial correlation. By substituting a local mean value there, the speckle noise is eliminated. In comparison to mean filters, adaptive mean filters function better and typically lessen speckles while maintaining edges.

In order to create a uniform histogram, the histogram equalisation technique relates to redistributing the grey levels. In this instance, the integral of the image's histogram is used to replace each pixel [16]. Histogram equalisation is a technique for adjusting contrast in image processing that makes use of the histogram of the image. The intensities on the histogram can be more evenly spread by making this adjustment. This makes it possible to improve contrast in places with lower local contrast. By effectively distributing the most frequent intensity values, histogram equalisation achieves this. The technique works well in pictures where the foreground and background are both dark or both bright.

Local contrast enhancement and histogram modification are processed in two stages by the Histogram Modified Local Contrast Enhancement (HM-LCE) approach [17]. The capability of this contrast boosting methodology has been significantly increased to the expected level, and this histogram adjusted LCE technique offers better image contrast boosting in terms of both subjective and objective quality.

The Contrast Limited Adaptive Histogram Equalization (CLAHE) technique, a specific case of the histogram equalisation technique that adapts to the image to be enhanced [18] , is used during the contrast enhancement phase. The CLAHE approach was initially created for medical imaging and aims to lessen the noise and edge shadowing effect caused in homogeneous areas.

For images that have been harmed by blur and additive noise, the Wiener filter is the Mean Squared Error (MSE) -best stationary linear filter. The signal and noise processes must be assumed to be second-order stationary in order to calculate the Wiener filter.

3. Methodology

The suggested framework is depicted in Fig. 1 and comprises of two preprocessing methods, one for the improvement of images and the other for the elimination of speckle noise in BUS images. The technique mostly consists of two phases:

1. Speckle noise reduction using Non-Local Means filter.

2. Image enhancement through the application of several morphological processes.

Because pixel values can range from 0 to 256, the image must be normalised. A color code is represented by each

digit. The computation of large numeric values may become more difficult when using the image as-is for additional processing. We can normalise the data to fall between 0 and 1 to lessen this.

The quality of images is lowered by speckle noise, a granular noise that is present in all images by nature. Spatial correlated multiplicative noise is used to mimic speckle noise[19]. At every level of the acquisition process, noise is added.

A crucial preprocessing step for the extraction of characteristics, analysis, and recognition from measurements of medical ultrasound images is speckle reduction. Since they eliminate the high frequencies and so tend to smooth off the edges of the image, commonly used linear low-pass filters, such the mean filters, are not ideal for reducing the speckle noise of ultrasound images.

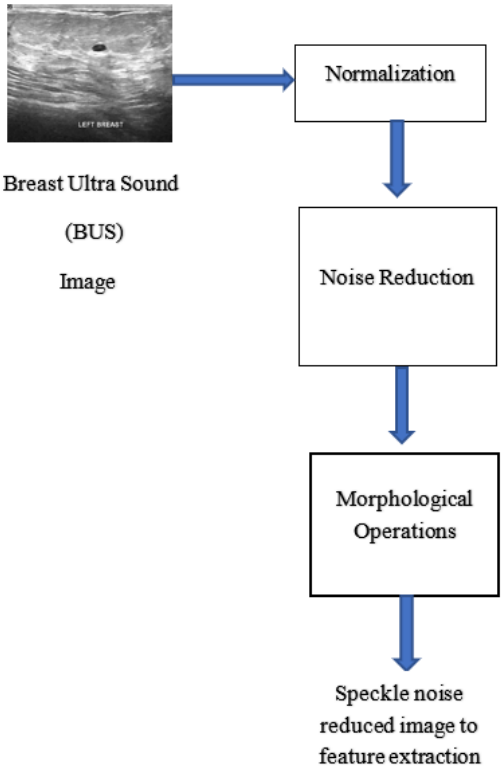

Fig – 1 : Proposed Method

Speckle impairs the clarity of ultrasound images and lessens a human observer's capacity to distinguish between minute details during a diagnostic examination.

Equation 2 provides the gamma distribution-following speckle noise as

$$F(g) = \frac{g^{\alpha-1} e^{g/a}}{(\alpha-1)!\, a^{\alpha}} \qquad (2)$$

where the variance is $a^2\alpha$ and g is the gray level. One of the spatial domain filters is the non-local means filter. In Non-local means filtering, a single pixel is reconstructed by averaging every observed pixel. A proposed the non-local means algorithm for noise removal by Buades et al. [20][21]. Given a discrete noisy image v = { $v(i) \mid i \in I$ }, the estimated value NL[v](i), for a pixel i is computed as a weighted average of all the pixels in the image and is stated as in Equation 3 as

$$\mathrm{NL[v](i)} = \sum_{j \in I} W(i,j) v(j) \qquad (3)$$

where the weights { w(i,j) }$_j$ depend on the similarity between the pixels i and j, and the conditions $0 \le w(i,j) \le 1$ and $\sum_j W(i,j) = 1$ are satisfied.

Two pixels i and j are similar if the intensity gray level vectors v(N_i) and v(N_j) are similar, where N_k denotes a square neighborhood of fixed size and centered at a pixel k. This similarity is measured as a decreasing function of the weighted Euclidean distance $\|v(N_i) - v(N_j)\|^2_{2,a}$, where a > 0 is the standard deviation of Gaussian kernel. When used in noisy neighbourhoods, the Euclidean distance raises the equality shown by Equation 4 as

$$\mathrm{E}\, \|v(N_i) - v(N_j)\|^2_{2,a} = \|u(N_i) - u(N_j)\|^2_{2,a} + 2\sigma^2 \qquad (4)$$

The weights are defined as

$w(i,j) = \frac{1}{z(i)} e^{\frac{\|v(N_i) - v(N_j)\|^2_{2,a}}{h^2}}$ where Z(i) is the normalizing constant

$$z(i) = \sum_j e^{\frac{\|v(N_i) - v(N_j)\|^2_{2,a}}{h^2}}$$

and the parameter h acts as a degree of filtering. It regulates the exponential function's decay, and as a result, weights' decline as a function of Euclidean distances. This

technique has the advantage of maintaining image details while denoising.

The next stage, a morphological process for image improvement, receives the speckle noise reduced BUS image. The mathematical morphology method uses an object's structural advantages. These methods abstract the components of an image and employ relationships between classes to describe the form of zones. They rely on mathematical ideas. The input for morphological operators is two sets of data, and they are non-linear. The original image is included in the main set, while the final one labels the structural component known as the mask. The mask will be a matrix of zeros and ones, whereas the original image is in the form of a binary or grey level. A new value for each and every pixel is obtained by sliding the mask on the original image after applying the final image to the morphological operators. Each mask's value one denotes efficacy, while its value zero denotes final image competencies. A mask can be created using the modified formats.

If S(p,q) and T(k,l) represents the gray-level image and the structural element matrices respectively, erosion and dilation operators are defined [22] as stated by Equations (5) and (6):

The erosion operator reduces the size of the objects but enlarges the holes in the image and removes the fine detail of that image. The finished image seems darker than the original image after bright regions below the mask are removed. The dilation operator performs in reverse, enlarging and contracting the size of image objects and holes. The closing operator performs in reverse as Equation 8, whereas the opening operator corresponds to the presentation of the erosion and dilation operations on the same image as Equation 7.

3.1 Data collection

The Breast Ultrasound Images Dataset from Kaggle is used for the experiment [23]. Breast ultrasound scans of women between the ages of 25 and 75 are part of the baseline data collection. This information was gathered in 2018. There are 600 female patients in all. With an average image size of 500x500 pixels, the collection comprises of 780 images. The majority of ultrasound (US) images are grayscale. At Baheya Hospital, they were gathered and kept in a DICOM format. The images were gathered and annotated over the course of about a year. The US dataset is divided into three categories: benign, malignant, and normal.

1100 images have been gathered up until that point. The dataset's number of images was halved to 780 images after preprocessing. The original images have insignificant information that cannot be categorised in bulk. Additionally, they could have an impact on the training process' output results. The LOGIQ E9 ultrasound system and the LOGIQ E9 Agile ultrasound system are the tools utilised in the scanning procedure. These tools are typically employed in high-quality imaging for applications in radiology, cardiology, and vascular care. They generate images with a 1280x1024 resolution. The ML6-15-D Matrix linear probe has 1e5 MHz transducers. PNG files make up the images.

4. Implementation

We compared the suggested method to different preprocessing methods in order to validate it. By employing multiple filtering approaches, the preprocessing technique used in this study effort reduces unnecessary noise and improves the image quality. This study employs a variety of image filtering algorithms, including Wiener, Mean, Median, Bilateral, Anisotropic Diffusion, Non-Local Means and Total Variation. The findings are studied and compared to a standard noise pattern, as well as rated in terms of quality. The goal of this study is to focus on selecting the proper

$$S\Theta T = min_{k,l}\{A(p+k, q+l) - T(k,l)\} \quad (5)$$

$$S \oplus T = \max_{k,l}\{S(p-k, q-1) + T(k,l)\} \quad (6)$$

filtering algorithms and reducing noise by taking into account the type of breast ultrasound images. The used preprocessing strategy not only saves time, but it also compares the seven types of filters and looks for the best

$$SoT = (S\Theta T) \oplus T \quad (7)$$

$$S \cdot T = (S \oplus T)\Theta T \quad (8)$$

pixel result using the Non-Local Means filter.

The approach was written in Python and tested on the Google Colab environment to speed up the process. A comparison of various filters for speckle noise reduction is carried out. The easiest way to compare preprocessing algorithms honestly is to set a benchmark and evaluate them using a widely accepted criterion. Unfortunately, there is very little published research in the field of medical image segmentation that compares different methods fairly.

Even if a method can generate promising results using its own database, it's difficult to say how good it is without peer comparison. As a result, we statistically assess the outcomes using numerous metrics (MSE, PSNR,SSIM,AMBE and SAM in this case), which quantify performance across multiple dimensions.

5. Results and Analysis

The method's implementation is tested on ten random BUS images. Various denoising filters were used, including Wiener filter without Fast Fourier Transform (FFT), Wiener with FFT, Mean filter, Median filter, Bilateral filter, Anisotropic Diffusion filter and Total Variation filter with the outcome indicating that the proposed method for speckle noise reduction outperforms all others.

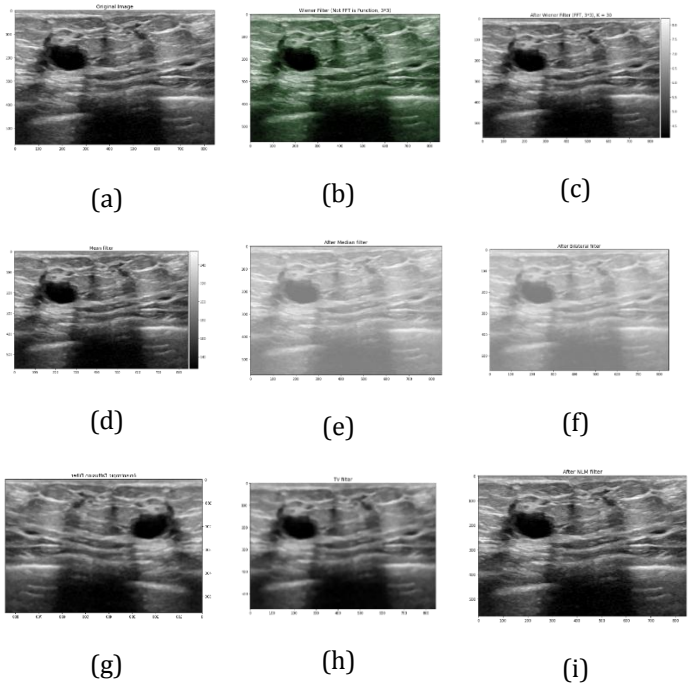

(a) (b) (c)

(d) (e) (f)

(g) (h) (i)

Fig 2.(a) Original BUS image (b) Wiener Filter without FFT (c) Wiener Filter with FFT

(d) Mean Filter (e) Median Filter (f) Bilateral Filter

(g) Anisotropic Diffusion Filter (h) TV Filter (i) NLM Filter

The original BUS image is displayed in Figure 2(a). The output of a Wiener Filter without FFT is shown in Figure 2(b), which uses a 3x3 kernel. The result of applying the Wiener filter with FFT is shown in Figure 2(c). After applying Mean Filter, the result is shown in Figure 2(d). The outcome of the Median Filter is shown in Fig 2(e). Figure 2(f) depicts the outcome of using the Bilateral filter, while Figure 2(g) depicts the result of using the Anisotropic Diffusion filter, Figure 2(h) portraits the result of Total Variation filter and Figure 2(i) shows the result of NLM filter.

The performance of several denoising filters is compared in Chart 1, and it is obvious from the graph plot that the NLM filter outperforms all others.

Chart 1: PSNR comparison of various denoising filters

5.1 Performance Metrics

One of the most essential criterion for denoising filters is the determination of performance metrics for image preprocessing algorithms. There are a variety of performance metrics that may be used to evaluate the effectiveness of a noise removal method; in this study, metrics including Mean Square Error (MSE), Peak Signal to Noise Ratio (PSNR), and Structural Similarity Index (SSIM) are employed.

(i) Mean Square Error

The Mean Square Error (MSE) is a popular performance indicator for determining image quality. It simply considers the difference between the pixel value and the deformed image, not the pixels in the surrounding area.

$$\frac{1}{MN}\sum_{y=1}^{M}\sum_{x=1}^{N}[I(x-y)-I'(x-y)]^2 \qquad (9)$$

MN is the image dimension, where I(x,y) is the original picture and I'(x,y) is the distorted image, according to Equation (9). The highest MSE number is 255, which indicates that the image is of very poor quality, while the lowest MSE value shows that the image is of great quality.

The comparison analysis based on Mean Squared Error (MSE) is shown in Table 1.

Sample Images	Wiener without FFT	Wiener with FFT	Mean	Median	Bilateral	Anisotropic Diffusion	Total Variation	NLM
Image1	0.004	0.42	18.5	23.3	36.8	0.0008	0.001	0.0009
Image2	0.002	0.37	11.1	16.3	27.4	0.0009	0.001	0.0001
Image3	0.005	0.46	9.8	15.4	27.4	0.0019	0.002	0.0006
Image4	0.002	0.37	16.6	17.4	32.3	0.0021	0.002	0.0002
Image5	0.004	0.46	11.8	14.6	23.9	0.0855	0.029	0.0001
Image6	0.002	0.36	12.16	15.3	27.2	0.0008	0.001	0.0001
Image7	0.005	0.47	16.7	24.1	36.5	0.0413	0.012	0.0001
Image8	0.004	0.42	18.1	23.1	35.9	0.0012	0.001	0.0001
Image9	0.005	0.46	8.5	14.9	25.3	0.0008	0.001	0.0002
Image10	0.004	0.46	11	15.7	25.9	0.0012	0.002	0.0006

Table 1: Comparative analysis of various denoising filters for the BUS Images (measure: MSE)

(ii) Peak Signal to Noise Ratio

The peak signal to noise ratio (PSNR) is a decibel-based ratio that compares the maximum signal power to the maximum noise power.

$$PSNR = 20 \log_{10}(MAX_i) - 10.\log_{10}(MSE) \quad (10)$$

From Equation (10), MAX_i is the possible number of pixel value. The comparison study using PSNR is shown in Table 2.

Sample Images	Wiener without FFT	Wiener with FFT	Mean	Median	Bilateral	Anisotropic Diffusion	Total Variation	NLM
Image1	23.82	3.55	35.25	34.25	32.26	30.7	29	70.01
Image2	27.3	4.18	37.61	35.93	33.67	30.4	28.4	69.03
Image3	22.05	2.95	37.77	35.8	33.29	27.1	26.6	90.93
Image4	25.33	3.82	35.47	35.27	32.59	26.8	26.3	65.41
Image5	23.55	3.3	37.31	36.38	34.24	10.7	15.3	88.23
Image6	24.66	3.52	36.39	35.39	32.89	30.8	28.7	73.8
Image7	22.8	3.07	35.73	34.13	32.34	13.8	18.9	69.63
Image8	23.84	3.52	35.29	34.22	32.29	29.1	27.8	68.8
Image9	22.58	3.24	38.72	36.27	33.96	30.7	28.8	88.4
Image10	24.06	3.38	37.67	36.14	33.97	29.1	27.9	66.83

Table 2: Comparative analysis of various denoising filters for the BUS Images (measure: PSNR)

(ii) Structural Similarity Index

The Structure Similarity Indicator (SSIM) is a quality assessment index that is based on the computation of three terms: brightness, contrast, and structural. As seen in Equation(11), the overall index is a multiplicative combination of the three terms,

$$SSIM(x,y) = [\, l(x,y) \,]^{\alpha} \cdot [\, c(x,y) \,]^{\beta} \cdot [\, s(x,y) \,]^{\gamma} \quad (11)$$

Where l(x,y) , c(x,y) and s(x,y) represents the luminanace, contrast and structural terms.

Sample Images	Wiener without FFT	Wiener with FFT	Mean	Median	Bilateral	Anisotropic Diffusion	Total Variation	NLM
Image1	0.9995	0.9397	0.9193	0.826	0.7379	0.9994	0.9998	1
Image2	0.9998	0.9468	0.9482	0.8918	0.8255	0.9991	0.9998	1
Image3	0.9993	0.9343	0.94	0.8776	0.7977	0.9994	0.9998	1
Image4	0.9997	0.946	0.9378	0.871	0.7947	0.9992	0.9998	1
Image5	0.9995	0.9354	0.9305	0.8692	0.8274	0.9998	0.9998	1
Image6	0.9997	0.9489	0.9368	0.8782	0.8063	0.9995	0.9998	1
Image7	0.9994	0.9326	0.9139	0.8174	0.7345	0.9994	0.9998	1
Image8	0.9995	0.9403	0.9203	0.8269	0.7425	0.9996	0.9998	1
Image9	0.9992	0.934	0.9404	0.8752	0.8043	0.9994	0.9998	1
Image10	0.9995	0.9359	0.9448	0.8967	0.8399	0.9994	0.9998	1

Table 3: Comparative analysis of various denoising filters for the BUS Images (measure: SSIM)

Table 3 shows the comparative analysis based on Structural Similarity Index (SSIM).

(iii) Absolute Mean Brightness Error (AMBE)

To judge the performance in keeping the original brightness, an objective measurement is proposed. The absolute difference between the input and output image's mean AMBE = E(X)-E(Y) is referred to as absolute mean brightness error (AMBE) and is defined as the absolute difference between the input and output image's mean. The input and output images are denoted by X and Y, respectively. A lower AMBE suggests that the brightness has been kept more effectively [24]. Table 4 shows the comparative analysis based on Absolute Mean Brightness Error (AMBE).

Sample Images	Wiener without FFT	Wiener with FFT	Mean	Median	Bilateral	Anisotropic Diffusion	Total Variation	NLM
Image1	0.052	0.172	0.0003	0.0496	0.0006	0.0002	0.0002	0.0005
Image2	0.061	0.180	0.0002	0.0580	0.0046	0.0005	0.0001	0.0006
Image3	0.063	0.181	0.0014	0.1604	0.0026	0.0009	0.0001	0.0002
Image4	0.064	0.183	0.0001	0.1682	0.0037	0.0005	0.0002	0.0008
Image5	0.047	0.157	0.0004	0.0964	0.0014	0.0005	0.0001	0.0003
Image6	0.048	0.169	0.0005	0.0487	0.0050	0.0001	0.0001	0.0006
Image7	0.056	0.188	0.0001	0.0385	0.0056	0.0001	0.0002	0.0001
Image8	0.028	0.155	0.0016	0.1557	0.0121	0.0002	0.0005	0.0004
Image9	0.057	0.176	0.0020	0.0589	0.0091	0.0004	0.0002	0.0006
Image10	0.041	0.163	0.0020	0.1157	0.0040	0.0009	0.0001	0.0008

Table 4: Comparative analysis of various denoising filters for the BUS Images (measure: AMBE)

(iv) Spectral Angle Mapper(SAM)

SAM calculates a spectral angle between two spectral vectors with the same origin to resolve spectral similarity. Equation (12) is used to calculate the length of a spectrum vector L_ρ

$$L_\rho = \sqrt{\frac{\sum_{\lambda=1}^{M} (\varepsilon_\lambda)^2}{M}} \quad (12)$$

The spectral angle (θ) is calculated as in Equation (13):

$$\theta = \cos^{-1}\left(\frac{\sum_{\lambda=1}^{M}\rho_\lambda\rho'_\lambda}{L_\rho L\rho'}\right) \quad (13)$$

where Lρ is the length of the endmember vector [25] and $L\rho'$ is the length of the modeled spectrum vector calculated using Equation. (12)

The error metric for SAM is the spectral angle. A modelled spectrum is categorised as belonging to the endmember class if its spectral angle is less than a user-defined threshold.

Sample Images	Wiener without FFT	Wiener with FFT	Mean	Median	Bilateral	Anisotropic Diffusion	Total Variation	NLM
Image1	1.638	1.159	0.357	89.785	89.779	3.579	4.421	0.020
Image2	1.550	1.134	0.367	89.786	89.780	3.843	4.898	0.012
Image3	1.837	1.457	0.532	89.787	89.783	4.524	4.929	0.044
Image4	1.790	1.493	0.552	89.791	89.788	4.699	5.066	0.027
Image5	2.361	1.297	0.462	89.720	89.716	11.215	7.768	0.013
Image6	1.714	1.168	0.372	89.773	89.765	3.954	5.054	0.031
Image7	1.278	1.143	0.344	89.806	89.802	6.468	2.976	0.006
Image8	2.944	1.519	0.522	89.753	89.742	8.074	9.640	0.124
Image9	1.591	1.031	0.373	89.774	89.770	3.696	4.624	0.013
Image10	2.001	1.286	0.494	89.747	89.741	5.060	5.963	0.033

Table 5: Comparative analysis of various denoising filters for the BUS Images (measure: SAM)

Table 5 shows the comparative analysis based on Spectral Angle Mapper(SAM).

5.2 Morphological Operations

The speckle denoised image of BUS is provided as input to various morphological processes for contast augmentation in the second phase. Image components that are important in the representation and description of region form are extracted using morphological techniques. Morphological operations are a set of basic tasks that are reliant on the geometry of the image. It's usually done with binary images. It requires two data sources, one of which is the input image and the other of which is the structuring component. Morphological operators use two inputs: an image and a structural component, which are subsequently combined using set operators. The items in the input image are processed based on the structuring component's encoded properties of the image's shape.

Opening is comparable to erosion in that it removes bright foreground pixels from the margins of foreground pixels regions. The operator's effect is to protect foreground pixels that are identical to the structuring component, or that can completely encapsulate the structuring component while removing all other foreground pixels. An image's internal noise is removed using the opening technique. The first step in the opening process is erosion, followed by dilation.

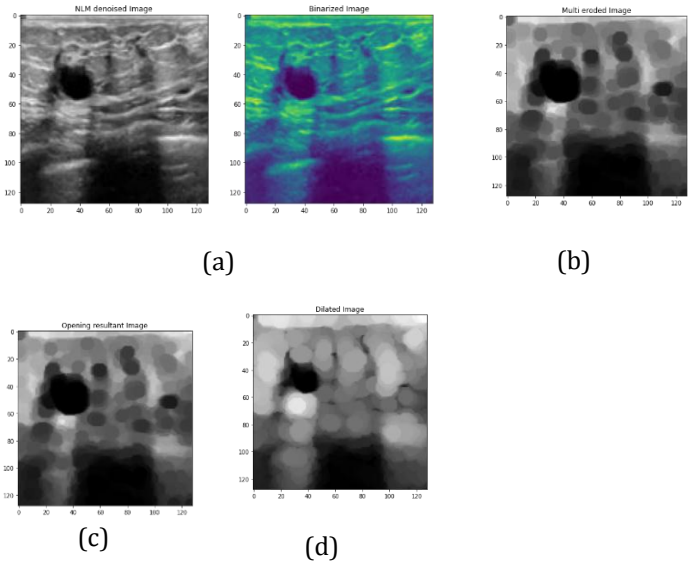

(a) (b) (c) (d)

Fig 3.(a) NLM denoised BUS image (b) Multi eroded image (c) Opening operation and Binarized image (d) Dilation operation

The NLM denoised image and its associated binarized image are shown in Figure 3(a). Figure 3(b) depicts the outcome of repeated erosion operations. The majority of superfluous artefacts and artefacts are eroded with successive erosion.

The result of the opening procedure, followed by erosion, is shown in Figure 3 (c). The remaining noise was removed using the opening procedure while the image's essential feature was preserved.

The size and shape of the artifacts have shrunk as a result of the successive erosion. Apply consecutive dilation with the same number of times erosion is applied to roughly recover their size. Furthermore, the same structuring element is used to ensure that the contour of the features is restored as closely as feasible to the original. The result of the dilation procedure is shown in Figure 3(d).

6. Conclusion

In this paper, we look into Breast Ultrasound image preprocessing and suggest a new framework for it. Two processes make up the proposed preprocessing method: speckle noise reduction and contrast enhancement. Many alternative speckle reduction strategies are investigated, and one is used as a preprocessing step in this study. The suggested method outperforms previous BUS image preprocessing methods utilising the same database, proving its superiority. Various performance measures are also investigated.

The following are some of the benefits of the proposed method:

1. It is entirely automated.

2. It also works nicely with low-contrast BUS images.

3. It outperforms other classic denoising filters and other picture enhancement approaches in terms of accuracy.

4. The proposed method takes roughly 20 seconds to analyse.

5. The proposed approach is quite stable.

7. Future Scope

The PSNR values of some BUS images were less than 50dB, which is a shortcoming of the suggested approach. This issue will be investigated more in the future. Another potential approach is to apply this technology to other applications like echocardiography and prostate ultrasonography, among others. Because this method is based on ultrasound imaging properties, it should be simple to adapt to various ultrasound images. The approach will also be used to segment and classify BUS images into normal, benign and malignant categories in the future.

References

1. Wein, W., Brunke, S., Khamene, A., Callstrom, M.R. and Navab, N., 2008. Automatic CT-ultrasound registration for diagnostic imaging and image-guided intervention. Medical image analysis, 12(5), pp.577-585.

2. Rundo, L., Militello, C., Vitabile, S., Russo, G., Sala, E. and Gilardi, M.C., 2020. A survey on nature-inspired medical image analysis: a step further in biomedical data integration. Fundamenta Informaticae, 171(1-4), pp.345-365.

3. Abd Ghani, M.K., Mohammed, M.A., Arunkumar, N., Mostafa, S.A., Ibrahim, D.A., Abdullah, M.K., Jaber, M.M., Abdulhay, E., Ramirez-Gonzalez, G. and Burhanuddin, M.A., 2020. Decision-level fusion scheme for nasopharyngeal carcinoma identification using machine learning techniques. Neural Computing and Applications, 32(3), pp.625-638.

4. Mohammed, M.A., Al-Khateeb, B., Rashid, A.N., Ibrahim, D.A., Abd Ghani, M.K. and Mostafa, S.A., 2018. Neural network and multi-fractal dimension features for breast cancer classification from ultrasound images. Computers \& Electrical Engineering, 70, pp.871-882.

5. Asgari Taghanaki, S., Abhishek, K., Cohen, J.P., Cohen-Adad, J. and Hamarneh, G., 2021. Deep semantic segmentation of natural and medical images: a review. Artificial Intelligence Review, 54(1), pp.137-178.

6. Mahapatra, D., Bozorgtabar, B. and Garnavi, R., 2019. Image super-resolution using progressive generative adversarial networks for medical image analysis. Computerized Medical Imaging and Graphics, 71, pp.30-39.

7. Arunkumar, N., Mohammed, M.A., Abd Ghani, M.K., Ibrahim, D.A., Abdulhay, E., Ramirez-Gonzalez, G. and de Albuquerque, V.H.C., 2019. K-means clustering and neural network for object detecting and identifying abnormality of brain tumor. Soft Computing, 23(19), pp.9083-9096.

8. Obaid, O.I., Mohammed, M.A., Ghani, M.K.A., Mostafa, A. and Taha, F., 2018. Evaluating the performance of machine learning techniques in the classification of Wisconsin Breast Cancer. International Journal of Engineering & Technology, 7(4.36), pp.160-166.

9. Arunkumar, N., Mohammed, M.A., Mostafa, S.A., Ibrahim, D.A., Rodrigues, J.J. and de Albuquerque, V.H.C., 2020. Fully automatic model-based segmentation and classification approach for MRI brain tumor using artificial neural networks. Concurrency and Computation: Practice and Experience, 32(1), p.e4962.

10. England, J.R. and Cheng, P.M., 2019. Artificial intelligence for medical image analysis: a guide for authors and reviewers. American journal of roentgenology, 212(3), pp.513-519.

11. Blum, D., Liepelt-Scarfone, I., Berg, D., Gasser, T., la Fougere, C. and Reimold, M., 2019. Controls-based denoising, a new approach for medical image analysis, improves prediction of conversion to Alzheimer's disease with FDG-PET. European Journal of Nuclear Medicine and Molecular Imaging, 46(11), pp.2370-2379.

12. Devarajan, G., Aatre, V.K. and Sridhar, C.S., 1991, January. Analysis of median filter. In ACE'90. Proceedings of [XVI Annual Convention and Exhibition of the IEEE In India] (pp. 274-276). IEEE.

13. Nagi, J., Kareem, S.A., Nagi, F. and Ahmed, S.K., 2010, November. Automated breast profile segmentation for ROI detection using digital mammograms. In 2010 IEEE EMBS conference on biomedical engineering and sciences (IECBES) (pp. 87-92). IEEE.

14. Cheng, H.D., Shan, J., Ju, W., Guo, Y. and Zhang, L., 2010. Automated breast cancer detection and classification using ultrasound images: A survey. Pattern recognition, 43(1), pp.299-317.

15. Maitra, I.K., Nag, S. and Bandyopadhyay, S.K., 2012. Technique for preprocessing of digital mammogram. Computer methods and programs in biomedicine, 107(2), pp.175-188.

16. Thangavel, K. and Roselin, R., 2009. Mammogram mining with genetic optimization of ant-miner parameters. International Journal of Recent Trends in Engineering, 2(3), p.67.

17. Sundaram, M., Ramar, K., Arumugam, N. and Prabin, G., 2011. Histogram modified local contrast enhancement for mammogram images. Applied soft computing, 11(8), pp.5809-5816.

18. Daskalakis, A., Cavouras, D., Bougioukos, P., Kostopoulos, S., Georgiadis, P., Kalatzis, I. and Nikiforidis, G., 2007, July. An efficient CLAHE-based, spot-adaptive, image segmentation technique for improving microarray genes' quantification. In 2nd International Conference on Experiments/Process/System Modelling/Simulation and Optimization.

19. Dass, R., 2018. Speckle noise reduction of ultrasound images using BFO cascaded with wiener filter and discrete wavelet transform in homomorphic region. Procedia computer science, 132, pp.1543-1551.

20. Wilson, B. and Das, J.P., 2013. A survey of non-local means based filters for image denoising. International Journal of Engineering Research & Technology, 2(10), pp.3768-3771.

21. Buades, A., Coll, B. and Morel, J.M., 2005. A review of image denoising algorithms, with a new one. Multiscale modeling & simulation, 4(2), pp.490-530.

22. Mehena, J., 2013. Medical images edge detection based on mathematical morphology. Journal of Computer and Communication Technology: Vol, 4(1), p.2.

23. Khaled, A.D.W.G.M., 2020. H Fahmy A. Dataset of breast ultrasound images Data Brief, 28(104863), pp.10-1016.

24. Chen, S.D. and Ramli, A.R., 2004. Preserving brightness in histogram equalization based contrast enhancement techniques. Digital Signal Processing, 14(5), pp.413-428.

25. Dennison, P.E., Halligan, K.Q. and Roberts, D.A., 2004. A comparison of error metrics and constraints for multiple endmember spectral mixture analysis and spectral angle mapper. Remote Sensing of Environment, 93(3), pp.359-367.